Journal of Materials Chemistry A

Accepted Manuscript

ROYAL SOCIETY OF CHEMISTRY

www.rsc.org/materialsA

Journal Name

ARTICLE

CdS-Phenanthroline Derivative Hybrid Cathode Interlayers for High Performance Inverted Organic Solar Cells

Received 00th January 20xx,
Accepted 00th January 20xx

DOI: 10.1039/x0xx00000x

www.rsc.org/

Xiaohui Liu,[†,a,b] Yulei Wu,[†,a] Xiaodong Li,[a,b] Wenjun Zhang,[a] Lixiao Zhao,[a] Hai-Qiao Wang*[,a] and Junfeng Fang*[,a]

Phenanthroline based organic seminconductors (BCP, Bphen, Mphen, Phen) are used to hybrid with CdS as cathode interlayers in inverted organic solar cells (OSCs). We observed that selecting the polar solvent and hydrophobic interlayers with diphenyl group could improve the performance of the organic photovoltaic devices. The modification to CdS can effectively improve its electrons mobility, film morphology, interfacial contact, and energy level alignment, which finally leads to the significantly enhancement of device performance. Through incorporating the hybrid CdS-P (CdS-BCP, CdS-Bphen, CdS-Mphen, CdS-Phen) as cathode buffer layer, the devices PCE (PTB7:$PC_{71}BM$ as active layer) is greatly improved from 3.09% to 8.36, 7.84, 6.69, 6.57% respectively, compared with device fabricated on the pristine CdS interlayer. These results indicate that the common inorganic semiconductor like CdS can be modified by some organic semiconductors to produce a general applicable electron transport layer applied in the OSCs. Our work puts forward new insights for the development of new interface modification material and fabrication of high efficiency devices.

Introduction

Solution-processed bulk heterojunction organic solar cells (OSCs) have attracted considerable attention due to their advantages of low cost, lightweight, flexibility and potential for large-scale manufacturing.[1-3] In the past decades, enormous progress has been achieved on improving the performance of OSCs and promising power conversion efficiency (PCE) of ~10% has been reported by several research groups based on different active blends.[4-8] To deliver a high power conversion efficiency for organic solar cells, besides active materials, the interfacial layers between active layer and electrodes play an important role as well.[9, 10] As the contact of the organic/electrode interface can significantly affect the parameters like open-circuit voltage (V_{oc}), short-circuit current (J_{sc}) and fill factor (FF) due to its abilities to tune the energy level alignment,[11, 12] improve the charge transporting at the interface,[13] promote the adhesion between electrode and active layer and enhance the light-trapping by optical spacer effect.[14, 15] Up to now, different p-/n- type interfacial materials including conjugate polyelectrolytes,[10, 16] crosslinkable materials,[17] small molecules,[18] inorganic materials like metal oxides,[19-21] and even ultra-thin/monolayer organic molecule modified metal oxides,[22-24] have been utilized in organic solar cells, and most of them can deliver fair device performance. However, challenges are still there and more efforts are needed in this field to promote the device performance.

Recently, as a further development of the thin organic molecule modifying interlayer strategy, a new type of organic-inorganic bulk-hybrid interlayer comes into the focus of this research field and some significant progresses have been made for the corresponding solar cells. These interlayers are composed of hybrid materials synthesized with corresponding organic and inorganic components hence they combine the advantages of both part like good conductivity and compatibility. In 2013, by using the Zn-C_{60} hybrid electron transport layer, Chen *et al.* achieved much improved performance for the P3HT:$IC_{60}BA$ (5.29% to 6.6%), PTB7:$PC_{71}BM$ (6.65% to 8.21%) and PTB7-Th:$PC_{71}BM$ (7.64% to 9.35%) blend-based devices, compared to the pristine ZnO interfacial layer device.[25] In 2014, they developed a new dual-doped ZnO interfacial material InZnO-BisC60, with which a new record PCE of 10.31% was achieved for single junction polymer solar cell based on the PTB7-Th:$PC_{71}BM$ blend with the same device architecture.[26] In the same year, similar functionality was demonstrated for poly(9, 9-bis-(6'-diethoxylphosphorylhexyl) fluorene) (PFEP) conjugated ZnO hybrid interlayer (ZnO-PFEP) in P(IID-DTC):$PC_{70}BM$ based polymer solar cells by Xie et al.[27] Promoted PCE up to 7.56% for ZnO-PFEP buffered device was achieved compared to the PCE of 5.24% with the pure ZnO interlayer device. Besides that, the conductive ZnO-PFEP allows a much larger thickness as

[a] Ningbo Institute of Materials Technology and Engineering, Chinese Academy of Sciences, Ningbo 315201, China. Email: hqwang@nimte.ac.cn, fangjf@nimte.ac.cn
[b] University of Chinese Academy of Sciences, Beijing 100049, China.

Electronic Supplementary Information (ESI) available: [Details of XPS spectra of CdS and CdS-BCP, *J*-*V* characteristics of OSCs based on various solvents with different concentrations, AFM height images of CdS-BCP with different solvents, EQE, absorption spectra, characteristic curves of electron-only devices, AFM height images of PTB7:$PC_{71}BM$ and UPS spectra]. See DOI: 10.1039/x0xx00000x

[†] Xiaohui Liu and Yulei Wu contributed equally to this work.

interfacial layer, benefiting the device reproducibility in large-scale printable technique. In our previous work, we also reported an organic-inorganic hybrid interfacial material CdS/2,9-Dimethyl-4,7-diphenyl-1,10-phenanthroline (CdS-BCP).[28] The hybrid chemical structure was demonstrated by the chemical bond between the two units verified by the X-ray photoelectron spectroscopy (XPS) analysis. As electron transporting layer, it delivered a high PCE of 7.47% for inverted PTB7:$PC_{71}BM$ device compared to the PCE of 4.77% and 6.57% of the reference devices with CdS and BCP as interlayer respectively, and improved very much the device stability compared to the conventional PEDOT:PSS buffered device. Furthermore, the hybrid-interlayer strategy has also been utilized in other type photovoltaics like perovskite solar cells and shown great potential.[29, 30] Although hybrid interfacial layers present promising potential in solar cells and remarkable improvements have been achieved. But still very limited work has been reported and most of them have focused on ZnO-based hybrid systems especially in organic solar cells. We believe it is worth to put more efforts in this hybrid interlayer technique to understand the underlying fundamental mechanism, explore and develop more efficient hybrid interlayers and even its application in other type photovoltaics.

Considering that BCP and 4,7-diphenyl-1,10-phenanthroline (Bphen) have been widely utilized in luminescent and photovoltaic devices as hole blocking/electron transport layer, excellent electrical properties of CdS inorganic semiconductor, and promising performance of the CdS-BCP hybrid interlayer solar cells achieved in our previous work, in this study, we systematically investigate the CdS-organic hybrid interlayer systems in PTB7:$PC_{71}BM$ solar cells. The phenanthroline and its derivatives Bphen, 2,9-dimethyl-1,10-phenanthroline (Mphen) and 1,10-phenanthroline (Phen)) are utilized as substitutes for BCP to modify CdS, forming hybrid interfacial materials CdS-Bphen, CdS-Mphen, and CdS-Phen. All of them outperform the pristine CdS when incorporated in the PTB7:$PC_{71}BM$ blend solar cells. And the CdS-BCP hybrid interlayer delivers the best power conversion efficiency of 8.36%.

Experimental

Materials and methods

$CdCl_2$, KS_2COEt and pyridine were bought from Aladdin Reagent. BCP, Bphen, Mphen and Phen were obtained from Alfa Aesar. PTB7 and $PC_{71}BM$ were purchased from 1-Material and ADS, respectively. All the available materials were used as received without any further purification.

The detailed preparation of Cadmium xanthate ($Cd(S_2COEt)_2$) was described in literatures.[28, 31] BCP was added into a stirring suspension solution of $Cd(S_2COEt)_2$ in chloroform. The suspension immediately changed to yellow solution after being stirred for 2 hours and then filtrated. The obtained clear filtrate was left to crystallize by slow evaporation of solvent. And then the crude product of $Cd(S_2COEt)_2$·(BCP) was purified by recrystallization from chloroform twice. $Cd(S_2COEt)_2$·(Bphen), $Cd(S_2COEt)_2$·(Mphen), $Cd(S_2COEt)_2$·(Phen), and $Cd(S_2COEt)_2$·$(C_5H_5N)_2$ crystals were prepared with the same route.

Device Fabrication

Pre-patterned indium tin oxide (ITO)-coated glass with a sheet resistance of 10 Ω per square was used as the substrate. It was cleaned by sequential sonication in detergent, deionized water, acetone, and isopropanol for 15 min at each step. After ultraviolet-ozone treatment for 30 min, the CdS-phenanthroline derivatives (CdS-P) precursors were spin-coated onto the ITO substrates at 5000 rpm and then annealed at 175 ^{o}C for 30 min. The thickness of the CdS-P layers and CdS layer after annealing were about 20 nm. Then the photoactive layer was deposited on top of the hybrid interlayers by spin-coating from the blend solution of PTB7:$PC_{71}BM$ dissolved in chlorobenzene/1,8-diiodoctane (97:3vol%) under 2000 rpm for 120 seconds, and the ratio of PTB7:$PC_{71}BM$ was 1:1.5 by weight (25 mg/ml). The device fabrication was finished by thermal evaporating a 10 nm MoO_3 layer and a 100 nm Al anode, at a vacuum level of 2×10^{-6} Torr. All the devices were fabricated under the same conditions and with an effective device area of 0.06 cm^2. The electron-only devices were made as the structure of ITO/ CdS or CdS-P/ PTB7:$PC_{71}BM$ /LiF /Al.

Characterization

J-V characteristics of photovoltaic cells were measured using a Keithley 2440 sourcemeter under the irradiation of a simulated AM1.5G solar spectrum with an Oriel Sol3A solar simulator. External quantum efficiency (EQE) was measured by using a Newport quantum efficiency measurement system (ORIEL IQE 200TM) with a lock-in amplifier and 150W xenon lamp under ambient atmosphere at room temperature. The light intensity at each wavelength was calibrated with a standard single-crystal Si/Ge photovoltaic cell.

Ultra-violet photoelectron spectroscopy (UPS) and XPS were performed using a Kratos AXIS ULTRA DLD XPS/UPS system. UPS was carried out using He I radiation at 21.21 eV from a discharge lamp operated at 20 mA, a pass energy of 5 eV, and a channel width of 25 meV. A -7.35 V bias was applied to the samples in order to separate the sample and analyzer low-kinetic-energy cutoffs. For XPS, survey scans to identify overall surface composition were carried out using a monochromatic Al Kα X-ray source (1486.6 eV). High-resolution scans to identify bonding states were performed at 20 eV pass energy and 50 meV channel width. All the spectra were adjusted according to the standard value of C 1s peak at 284.8 eV. The surface morphology of the hybrid buffer layers were investigated using a field-emission scanning electron microscope (FE-SEM) (Hitachi S-4800). Droplet images were recorded on a contact-angle system (model OCA20) and the film thickness was measured under Veeco Dektak 150.

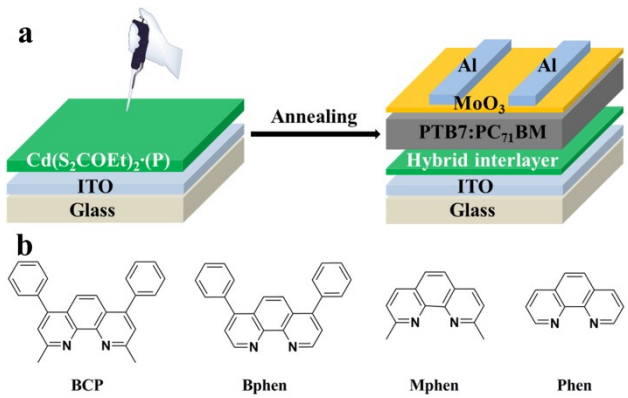

Fig. 1 (a) Device structure of the inverted OSCs fabricated with different CdS-P hybrid interlayers, and (b) the molecular structures of BCP, Bphen, Mphen and Phen.

Results and discussion

In our previous work, based on the solution-processable precursor $Cd(S_2COEt)_2$·(BCP) (dissolved in acetone, 10mg/mL), hybrid CdS-BCP cathode interlayer was prepared by thermal annealing. The hybrid molecule structure was confirmed by the chemical bond of Cd-N verified by the XPS analysis (Fig. S1). And power conversion efficiency of 7.47% has been achieved in inverted OSCs.[28]

To further investigate this hybrid interlayer system and optimize the device performance, in this study, we firstly investigated the influence of the solvent on the hybrid interlayer. Various polar solvents like chloroform (CF), acetone (AT), tetrahydrofuran (THF), and N,N-Dimethylformamide (DMF) with concentration gradients of 10 mg/mL, 20 mg/mL, and 30 mg/mL were applied to fabricate the hybrid interlayer CdS-BCP. Fig. S2 presents the current-voltage (*J*-V) characteristics of the obtained OSCs measured under AM 1.5G irradiation. The detailed parameters including short circuit current density (J_{sc}), open circuit voltage (V_{oc}), fill factor (FF) and PCE are summarized in Table S1. When processed by acetone with concentration of 10 mg/mL, the CdS-BCP hybrid interlayer delivered a PCE of 7.46%, with V_{oc} of 0.709 V, J_{sc} of 16.81 mA·cm^{-2} and FF of 62.58%, which is consistent with our previously reported results.[28] Obviously, processed with higher polar solvents (DMF, THF, AT), the hybrid interlayers deliver comparatively superior performances than that spin-cast from non-polar solvent CF. In more details, the polar solvent DMF processed hybrid interlayer elevated the device performance to 7.76%, compared with AT (7.46%) with the same concentration of 10 mg/mL, probably due to the higher boiling point and slower evaporation speed of DMF than that of AT, leading to better film morphology, hence better device performance (Fig. S3).

Hence we chose the optimal solvent DMF to process all the different CdS-Phenanthroline/derivative hybrid interlayers with fixed concentration of 10 mg/mL. Here, besides BCP, the organic part such as Bphen, Mphen and Phen are selected to coordinate with $Cd(S_2COEt)_2$ to prepare cadmium chelate compound precursors $Cd(S_2COEt)_2$·(P) (P: BCP, Bphen, Mphen and Phen). The inverted OSCs configuration studied in this work and the molecular structure of BCP, Bphen, Mphen and Phen are shown in Fig. 1. The crystals of $Cd(S_2COEt)_2$·(P) are formed by slow evaporation of CF and purified by recrystallization twice. And the acquired precursors $Cd(S_2COEt)_2$·(P) were dissolved in DMF with a concentration of 10 mg/mL and spin-cast at 5000 rpm onto the ITO surface and annealed at 175 °C for 30 minutes to form the CdS-P hybrid electron transport interlayer, as depicted in Fig. 1. The characteristic *J*-V curves of the optimized OSCs with device structure of ITO/CdS-P/PTB7:$PC_{71}BM$ /MoO_3 /Al, are presented in Fig. 2a and Table 1. For comparison, a control device with the interlayer of pristine CdS decomposed from its precursor $Cd(S_2COEt)_2$·(Pyridine)$_2$ was fabricated and tested as well. The devices based on the hybrid materials of CdS-BCP exhibit the best performance, with PCE increased from 3.09% to 8.36%, and the main parameters of V_{oc}, J_{sc} and FF improved from 0.404 V, 15.27 mA·cm^{-2}, and 50.13% to 0.722 V, 17.42 mA·cm^{-2}, and 66.44% respectively, compared to that with CdS. The CdS-Bphen devices present remarkably increased performance as well relative to that with CdS, with PCE increased from 3.09%

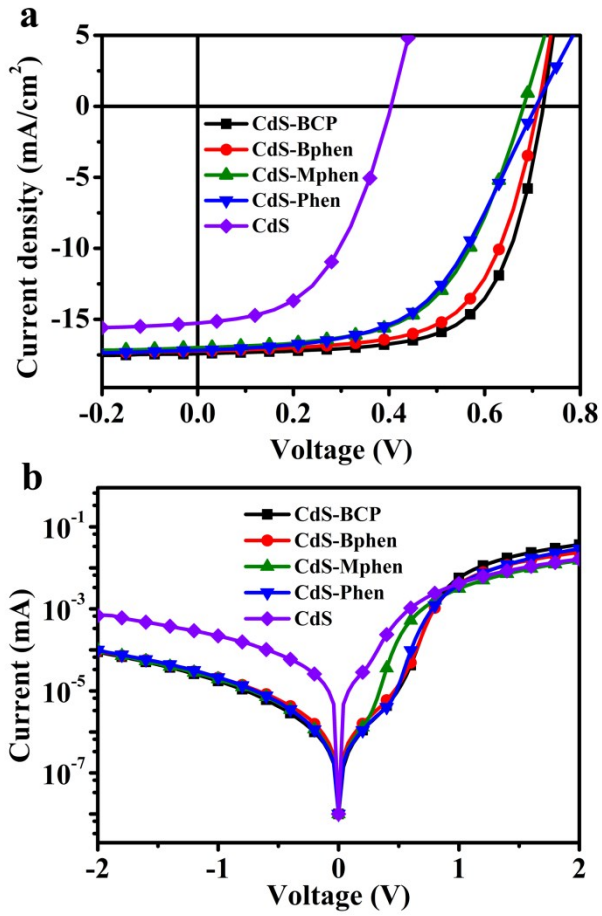

Fig. 2 (a) Illuminated and (b) dark *J*–V characteristic curves of devices, with architecture of ITO/Interlayer/PTB7:$PC_{71}BM$/ MoO_3/Al and with hybrid CdS-P or pure CdS as the interlayer.

Table 1 Performance of devices fabricated based on CdS or CdS-P as cathode buffer layer.

Interlayer	V_{oc}	J_{sc}	FF	PCE	R_s	R_{sh}
	V	mA·cm^{-2}	%	Best(Avg)	Ω·cm^2	KΩ·cm^2
CdS-BCP	0.722	17.42	66.44	8.36(8.23)	4.21	1.04
CdS-Bphen	0.711	17.23	64.02	7.84(7.72)	6.17	2.23
CdS-Mphen	0.681	16.98	57.86	6.69(6.55)	9.30	0.85
CdS-Phen	0.707	17.19	54.08	6.57(6.49)	14.74	0.88
CdS	0.404	15.27	50.13	3.09(2.96)	7.43	0.31

to 7.84%. Besides that, V_{oc}, J_{sc}, and FF are raised by 76%, 12.8%, and 27.7%, respectively. While for the devices fabricated with CdS-Mphen and CdS-Phen, relatively lower performances are obtained. As presented in the Table 1, relative low series resistances (R_s) and high shunt resistances (R_{sh}) are determined for the CdS-Bphen and CdS-BCP devices compared to the other hybrid and pure CdS interlayer devices, due to their different interfacial properties as their different organic ligands, which is consistent with their corresponding obtained performance parameters (Fig. 2a).

Fig. 2b presents the dark *J*-*V* curves of the devices. With hybrid interlayers, the devices exhibit a turn-on voltage of about 0.7~0.8 V while it is only 0.5~0.6 V for the CdS interlayer device, suggesting the built-in potential across the device, which is the upper limit of the attainable V_{oc} in OSCs,[32] and considerably increases upon utilization of the hybrid cathode interlayers. In addition, the leakage current in the devices with hybrid interlayers is significantly restrained, and the diode rectification ratio characterized at ± 2.0 V is 2~3 orders higher than that of the control device, indicating a greatly suppressed carrier recombination.[33] Obviously, hole blocking and electron collecting become more efficient when the hybrid CdS-P cathode buffer layers are used. Thus, higher photocurrent is accomplished by using hybrid interlayers. Furthermore, the hybrid interlayer devices show higher EQE value in average than that of the CdS based device in the wavelength range between 350 and 700 nm (Fig. S4), which could have been resulted from the more efficient electron transport and collection at the electrode after modification of the CdS by organic ligands, since no obvious contribution derived from interlayer absorption to the photocurrent are observed as demonstrated by the absorption spectra of devices with CdS-BCP or CdS interlayer (Fig. S5).

To evaluate the charge carrier mobility in the devices incorporated with the hybrid interlayers CdS-P, the apparent charge transport mobilities were tested by using electron-only devices with structure of ITO/CdS or CdS-P /PTB7:$PC_{71}BM$ /LiF /Al (Fig. S6), according to the space charge limited current (SCLC) model (Fig. 3).[25, 32, 34] As fitted by the SCLC model,

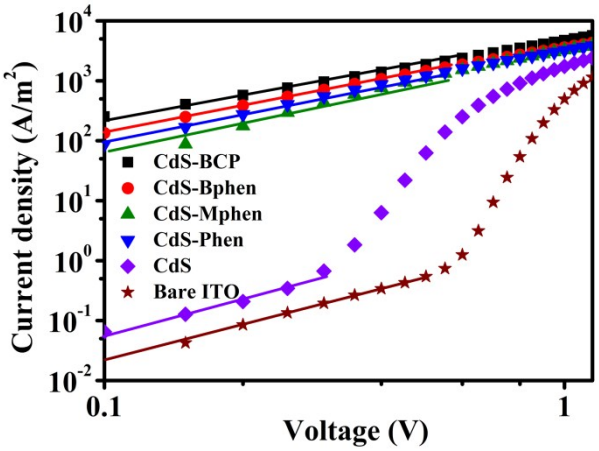

Fig. 3 Fitting results by using SCLC model (log scale). The electron mobility was obtained from the Mott–Gurney space-charge-limited current (SCLC) equation: $J = 9\,\varepsilon_r\,\varepsilon\,\mu\,V^2/(8d^3)$, where J is the current density, μ is the apparent charge carrier mobility, which includes the effect of transport efficiency or traps, ε is the permittivity of free space, ε_r is the relative permittivity of the medium, V is the applied voltage, and d is the thickness of the active layer.

apparent electron mobilities are determined to be 3.42×10^{-3}, 2.58×10^{-3}, 1.37×10^{-3}, 1.80×10^{-3} cm^2·V^{-1}·s^{-1} for CdS-BCP, CdS-Bphen, CdS-Mphen, and CdS-Phen based devices, which are three orders of magnitude compared to that of the pristine CdS interlayer devices (1.61×10^{-6} cm^2·V^{-1}·s^{-1}). And this enhanced charge carrier mobility could account for the J_{sc} improvement of the hybrid interlayer based devices compared to the CdS based device.

In addition, the surface morphologies of CdS and different hybrid interfacial films were investigated by SEM, as displayed in Fig. 4. The CdS film presents island shape morphology when deposited on bare ITO substrate as shown in Fig. 4e. While the BCP and Bphen modified CdS film show dense black dots (in the scale of 10 μm) well-distributed on the surface of ITO (Fig. 4a, b), and the CdS-Mphen and CdS-Phen films show reticulated surface morphology on ITO (Fig. 4c, d), all of which are distinct from the pure CdS film. The difference in surface morphology of the different hybrid CdS-P films could partly explain for the different improvement of their performance,[35-37] indicating that these hybrid CdS-P films can play an important role in delivering a high device performance. Furthermore, we conducted the AFM test in a tapping mode

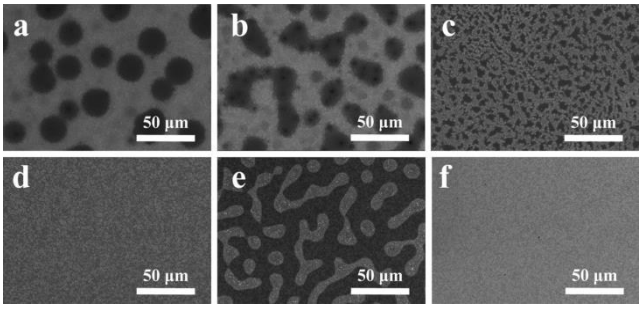

Fig. 4 SEM images of different hybrid cathode interlayer coated ITO. (a) CdS-BCP, (b) CdS-Bphen, (c) CdS-Mphen, (d) CdS-Phen, (e) CdS, and (f) Bare ITO.

for the pothoactive layer (PTB7:$PC_{71}BM$) on different hybrid interlayers (Fig. S7). The PTB7:$PC_{71}BM$ films on top of CdS-BCP, CdS-Bphen and CdS-Phen hybrid interlayers exhibit similar smoother surface and better phase separation compared to the active layer on CdS film, which is consistent with the obtained device performances.

Aggregates of the hybrid materials deposited on ITO substrate are considered to be chelate compounds i.e. CdS-BCP, CdS-Bphen, CdS-Mphen and CdS-Phen, in which CdS is still coordinating with BCP, Bphen, Mphen and Phen, respectively, when decomposed from their precursors at 175 ^{o}C. As BCP (/Bphen/Mphen/Phen) is a bidentate ligand and two nitrogen atoms of which can bond to Cd atom, the hydrophilic nature of CdS film is thence changed after modification by different organic ligands (Fig. 5). In the hybrid films, nitrogen atoms possess higher electronegativity thus chelate the CdS closely while the aromatic ring will orient upwards as its lower electronegativity, which makes the film hydrophobic and compatible with nonpolar chlorobenzene solvent. This is consistent with the results of the water contact angle measurements (Fig. 5). Especially, in the film of CdS-BCP and CdS-Bphen (Fig. 5a, b), the existence of diphenyl group makes it more hydrophobic than the CdS-Mphen and CdS-Phen (Fig. 5c, d).[34] The bare ITO with a contact angle of 12^{o} is displayed in Fig. 5f for comparison. The water contact angle increases from 54^{o} of the pristine CdS to 78^{o}, 76^{o}, 60^{o} and 66^{o} of the CdS-BCP, CdS-Bphen, CdS-Mphen and CdS-Phen films, respectively. The results confirm the more hydrophobic property of the hybrid CdS-P surface, which is consistent with the results of the SEM analysis. In brief, these hybrid interfacial layers by organic ligands modification can increase the interfacial intimate contact with photoactive layer, benefiting the device performance.

Moreover, for high performance OSCs, well-matched energy levels between the CdS-P interlayer modified electrode and the photoactive layer are required. Fig. 6 shows the energy level diagrams of the materials used in this work according to the studies of UPS measurement (Fig. S8) and reported scientific literatures.[38, 39] The work function of bare ITO is measured to be -4.4 eV while the LUMO of $PC_{71}BM$ is -3.69 eV. After modification by CdS or hybrid CdS-P, the work functions are effectively decreased to -4.17 eV and -3.97, -4.09, -3.85, -3.81 eV, respectively, due to the introduced different

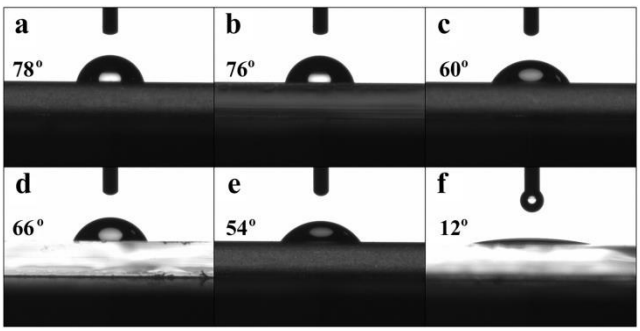

Fig. 5 Water contact angle images of (a) CdS-BCP 78^{o}, (b) CdS-Bphen 76^{o}, (c) CdS-Mphen 60^{o}, (d) CdS-Phen 66^{o}, (e) CdS 54^{o} and (f) Bare ITO 12^{o}.

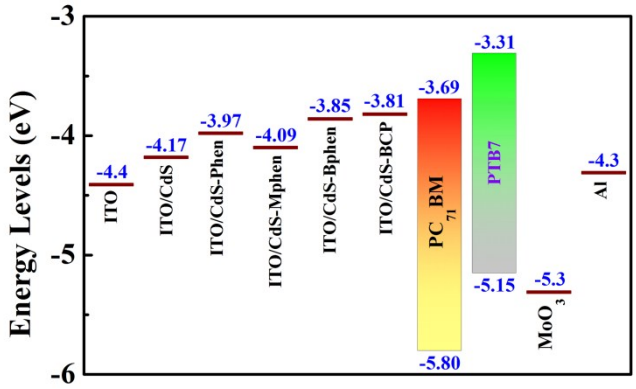

Fig. 6 Energy level diagrams of materials used in the inverted devices fabrication.

electronic dipoles by their different molecule polarity,[35, 40, 41] which are more comparable to the LUMO of $PC_{71}BM$. Hence, electrons can be more facilely transferred from the LUMO of $PC_{71}BM$ to the ITO electrode through the interlayers and to be collected more efficiently. Furthermore, the V_{oc} of devices fabricated with CdS or hybrid CdS-P interlayers would be related to the variation of their work functions. However, the V_{oc} can also be influenced by the different work functions of the two electrodes when the interfaces between active layer and electrodes are non-ohmic contacts.[42, 43] In our study, the V_{oc} of the inverted solar cells is dependent on the work functions of the cathode interlayers. The decreased effective work functions of hybrid cathode buffer layers can lead to larger build-in potentials, and that is the upper limit of the attainable V_{oc} in devices as described above. Therefore, the V_{oc} of devices based on CdS-BCP, CdS-Bphen, CdS-Mphen and CdS-Phen interlayers increases to 0.722, 0.711, 0.681 and 0.707V, respectively, compared to 0.404 V of the CdS-based device. The decreased effective work functions of CdS-P films may be attributed to the fill-up of CdS surface traps by phenanthroline and its derivatives, which would greatly decrease the possible trap-assisted interfacial charge recombination. In addition, the energy-level adjustment by hybrid CdS-P interlayer become more facile for electron extraction, which is consistent with a large forward current and a large photocurrent and can explain for the trend of J_{sc}, eventually leading to high performance of OSCs.

Conclusions

In summary, we fabricated inverted organic solar cells by using homologous hybrid materials CdS-BCP, CdS-Bphen, CdS-Mphen and CdS-Phen as the electron transporting layer. High polarity and boiling point solvent, DMF is selected to process the hybrid interfacial layers as it is ability to improve the interface properties and enhance device performance. The influences of different organic ligands (BCP, Bphen, Mphen, Phen) on the performance of the inverted OSCs were investigated comprehensively. Modification of the CdS with organic ligands, effectively improved the electron mobility,

film morphology, interfacial contact, and energy alignment, eventually leading to the enormous enhancement of device performance, with PCE improved from 3.09% to 8.36, 7.84, 6.69, 6.57% respectively. And the hybrid interlayers with hydrophobic diphenyl group (CdS-BCP and CdS-Bphen) is favorable to fabricate high performance device. These results indicate that the strategy of hybridization of conventional inorganic and organic semiconductor could produce promising charge carrier transporting material for organic optoelectronic devices.

Acknowledgements

The Project was supported by National Natural Science Foundation of China (51273208, 61474125, 51502313), and Zhejiang Provincial Natural Science Foundation of China (LR14E030002) and Ningbo City Natural Science Foundation of China (2014A610037); The work was also supported by Hundred Talent Program of Chinese Academy of Sciences. We also thanked the support of Jiangsu Collaborative Innovation Center of Photovoltaic Science and Engineering (Changzhou, 213164, P.R.China).

Notes and references

1 G. Li, R. Zhu and Y. Yang, *Nat. Photonics*, 2012, **6**, 153-161.
2 B. C. Thompson and J. M. J. Fréchet, *Angew. Chem. Int. Ed.*, 2008, **47**, 58-77.
3 L. Ye, S. Zhang, L. Huo, M. Zhang and J. Hou, *Acc. Chem. Res.*, 2014, **47**, 1595-1603.
4 Z. He, B. Xiao, F. Liu, H. Wu, Y. Yang, S. Xiao, C. Wang, T. P. Russell and Y. Cao, *Nat. Photonics*, 2015, **9**, 174-179.
5 L. K. Jagadamma, M. Al‐Senani, A. El‐Labban, I. Gereige, N. Ndjawa, O. Guy, J. C. Faria, T. Kim, K. Zhao and F. Cruciani, *Adv. Energy Mater.*, 2015, **5**, 1500204.
6 S. Zhang, L. Ye, W. Zhao, B. Yang, Q. Wang and J. Hou, *Sci. China Chem.*, 2015, **58**, 248-256.
7 J. Kong, I. W. Hwang and K. Lee, *Adv. Mater.*, 2014, **26**, 6275-6283.
8 Y. Liu, J. Zhao, Z. Li, C. Mu, W. Ma, H. Hu, K. Jiang, H. Lin, H. Ade and H. Yan, *Nat. Commun.*, 2014, **5**, 5293.
9 C.-C. Chueh, C.-Z. Li and A. K.-Y. Jen, *Energy Environ. Sci.*, 2015, **8**, 1160-1189.
10 Z. He, C. Zhong, S. Su, M. Xu, H. Wu and Y. Cao, *Nat. Photonics*, 2012, **6**, 591-595.
11 R. Xia, D. S. Leem, T. Kirchartz, S. Spencer, C. Murphy, Z. He, H. Wu, S. Su, Y. Cao and J. S. Kim, *Adv. Energy Mater.*, 2013, **3**, 718-723.
12 W. E. Ford, D. Gao, N. Knorr, R. Wirtz, F. Scholz, Z. Karipidou, K. Ogasawara, S. Rosselli, V. Rodin and G. Nelles, *ACS nano*, 2014, **8**, 9173-9180.
13 T. M. Clarke and J. R. Durrant, *Chem. Rev.*, 2010, **110**, 6736-6767.
14 A. Hadipour, D. Cheyns, P. Heremans and B. P. Rand, *Adv. Energy Mater.*, 2011, **1**, 930-935.
15 A. K. K. Kyaw, D. H. Wang, D. Wynands, J. Zhang, T.-Q. Nguyen, G. C. Bazan and A. J. Heeger, *Nano Lett.*, 2013, **13**, 3796-3801.
16 J. H. Seo, A. Gutacker, Y. Sun, H. Wu, F. Huang, Y. Cao, U. Scherf, A. J. Heeger and G. C. Bazan, *J. Am. Chem. Soc.*, 2011, **133**, 8416-8419.
17 Y. Sun, S.-C. Chien, H.-L. Yip, Y. Zhang, K.-S. Chen, D. F. Zeigler, F.-C. Chen, B. Lin and A. K.-Y. Jen, *Chem. Mater.*, 2011, **23**, 5006-5015.
18 W. Zhang, Y. Wu, Q. Bao, F. Gao and J. Fang, *Adv. Energy Mater.*, 2014, **4**, 1400359.
19 Z. a. Tan, W. Zhang, Z. Zhang, D. Qian, Y. Huang, J. Hou and Y. Li, *Adv. Mater.*, 2012, **24**, 1476-1481.
20 Y. Sun, J. H. Seo, C. J. Takacs, J. Seifter and A. J. Heeger, *Adv. Mater.*, 2011, **23**, 1679-1683.
21 M. D. Irwin, D. B. Buchholz, A. W. Hains, R. P. Chang and T. J. Marks, *Proc. Natl. Acad. Sci.*, 2008, **105**, 2783-2787.
22 T. Stubhan, M. Salinas, A. Ebel, F. C. Krebs, A. Hirsch, M. Halik and C. J. Brabec, *Adv. Energy Mater.*, 2012, **2**, 532-535.
23 H. Choi, J. S. Park, E. Jeong, G. H. Kim, B. R. Lee, S. O. Kim, M. H. Song, H. Y. Woo and J. Y. Kim, *Adv. Mater.*, 2011, **23**, 2759-2763.
24 Y. Zhou, C. Fuentes-Hernandez, J. Shim, J. Meyer, A. J. Giordano, H. Li, P. Winget, T. Papadopoulos, H. Cheun and J. Kim, *Science*, 2012, **336**, 327-332.
25 S. H. Liao, H. J. Jhuo, Y. S. Cheng and S. A. Chen, *Adv. Mater.*, 2013, **25**, 4766-4771.
26 S.-H. Liao, H.-J. Jhuo, P.-N. Yeh, Y.-S. Cheng, Y.-L. Li, Y.-H. Lee, S. Sharma and S.-A. Chen, *Sci. Rep.*, 2014, **4**. 6813.
27 J. Liu, J. Wu, S. Shao, Y. Deng, B. Meng, Z. Xie, Y. Geng, L. Wang and F. Zhang, *ACS Appl. Mater. Interfaces*, 2014, **6**, 8237-8245.
28 Y. Wu, W. Zhang, X. Li, C. Min, T. Jiu, Y. Zhu, N. Dai and J. Fang, *ACS Appl. Mater. Interfaces*, 2013, **5**, 10428-10432.
29 L. Zuo, Z. Gu, T. Ye, W. Fu, G. Wu, H. Li and H. Chen, *J. Am. Chem. Soc.*, 2015, **137**, 2674-2679.
30 W. Chen, Y. Wu, J. Liu, C. Qin, X. Yang, A. Islam, Y.-B. Cheng and L. Han, *Energy Environ. Sci.*, 2015, **8**, 629-640.
31 V. Varand, L. Glinskaya, R. Klevtsova and S. Larionov, *J. Struct. Chem+.* 1998, **39**, 244-252.
32 Z. He, C. Zhong, X. Huang, W. Y. Wong, H. Wu, L. Chen, S. Su and Y. Cao, *Adv. Mater.*, 2011, **23**, 4636-4643.
33 V. Mihailetchi, P. Blom, J. Hummelen and M. Rispens, *J. Appl. Phys.*, 2003, **94**, 6849-6854.
34 B. R. Lee, E. D. Jung, Y. S. Nam, M. Jung, J. S. Park, S. Lee, H. Choi, S. J. Ko, N. R. Shin and Y. K. Kim, *Adv. Mater.*, 2014, **26**, 494-500.
35 Antoine Kahn, *Mater. Horiz.*, 2015, DOI: 10.1039/C5MH00160A.
36 R. Steim, F. R. Kogler and C. J. Brabec, *J. Mater. Chem.*, 2010, **20**, 2499-2512.
37 M. Gräetzel, R. A. Janssen, D. B. Mitzi and E. H. Sargent, *Nature*, 2012, **488**, 304-312.
38 C. Tao, S. Ruan, X. Zhang, G. Xie, L. Shen, X. Kong, W. Dong, C. Liu and W. Chen, *Appl. Phys. Lett.*, 2008, **93**, 193307-1-193307-3.
39 Y. Liang, Z. Xu, J. Xia, S. T. Tsai, Y. Wu, G. Li, C. Ray and L. Yu, *Adv. Mater.*, 2010, **22**, E135-E138.
40 R. T. Tung, *Phys. Rev. B*, 2001, **64**, 205310.
41 X. Crispin, V. Geskin, A. Crispin, J. Cornil, R. Lazzaroni, W. R. Salaneck and J.-L. Bredas, *J. Am. Chem. Soc.*, 2002, **124**, 8131-8141.
42 J. Liu, S. Shao, G. Fang, B. Meng, Z. Xie and L. Wang, *Adv. Mater.*, 2012, **24**, 2774-2779.
43 H.-H. Liao, L.-M. Chen, Z. Xu, G. Li and Y. Yang, *Appl. Phys. Lett.*, 2008, **92**, 173303.

TOC graphic

High performance inverted OSCs were achieved by using hybrid CdS-Phenanthroline derivative as the electron transporting layer through thermal decomposition.